

A&A manuscript no.

(will be inserted by hand later)

Your thesaurus codes are:

03 (13.09.3); (13.09.4); (11.09.1 M 82); (11.09.1 NGC 253); (11.09.1 Circinus); (11.09.1 NGC 1068)

ASTRONOMY  
AND  
ASTROPHYSICS

# ISO-SWS spectra of galaxies: continuum and features <sup>★</sup>

E. Sturm<sup>1,2</sup>, D. Lutz<sup>1</sup>, D. Tran<sup>1</sup>, H. Feuchtgruber<sup>1</sup>, R. Genzel<sup>1</sup>, D. Kunze<sup>1</sup>, A.F.M. Moorwood<sup>3</sup>, and M.D. Thornley<sup>4</sup>

<sup>1</sup> Max-Planck-Institut für extraterrestrische Physik, Postfach 1603, D-85740 Garching, Germany

<sup>2</sup> Infrared Processing and Analysis Center, MS 100-22, Pasadena, CA 91125, USA

<sup>3</sup> European Southern Observatory, Karl-Schwarzschild-Str. 2, D-85748 Garching, Germany

<sup>4</sup> National Radio Astronomy Observatory, 520 Edgemont Road, Charlottesville, VA 22903, USA

Received 19 October 1999 / Accepted 26 January 2000

**Abstract.** We present an inventory of mid-infrared spectral features detected in high resolution ( $R \sim 1500$ ) ISO-SWS 2.4–45  $\mu\text{m}$  spectra of the galaxies M 82, NGC 253, Circinus, NGC 1068, and a position in the 30 Doradus region of the Large Magellanic Cloud. We discuss their identifications and highlight possible relations between these features and the physical state of the interstellar medium in galaxies. The spectral features vary considerably from source to source in presence and relative strength. Emission features are largely absent in the intense radiation field close to an AGN. Compared to normal infrared-selected starbursts, they also seem to be weaker in a low metallicity, intensely star forming environment. The large number of features beyond 13  $\mu\text{m}$  is remarkable. Some of the features have – to our knowledge – not been reported before in astronomical objects.

In the 5–13  $\mu\text{m}$  region, emission from unidentified infrared bands (UIBs), usually ascribed to aromatic molecules, and apparent silicate absorption dominate the spectrum. The density of features makes it difficult to determine the continuum, particularly in ground-based data of limited wavelength coverage. In fact the apparent depth of the 9.7  $\mu\text{m}$  silicate absorption may be overestimated in the presence of UIB emission, as we demonstrate by comparing the spectrum of M 82 to the (absorption free) spectrum of the reflection nebula NGC 7023. No strong silicate absorption is present in M 82. The (very small grain) dust continuum under the UIB emission in our starburst templates can be modeled by a simple power law, starting at wavelengths between 8 and 9  $\mu\text{m}$ .

We find broad H<sub>2</sub>O-ice absorption features at 3.0  $\mu\text{m}$  in M 82 and NGC 253. Their optical depths (relative to the visual extinction) indicate that the lines of sight towards these galaxies have similar properties as the line of sight towards the Galactic Center. The active galaxy

NGC 1068 exhibits a clearly different spectrum of absorption features, indicating different physical conditions in the obscuring regions of this AGN compared to the starburst templates.

The spectra are valuable templates for future mid-infrared missions. We smooth our data to simulate low resolution spectra as obtained with ISOCAM-CVF, ISOPHOT-S, and in the future with the low resolution mode of SIRTIF-IRS, and use our high spectral resolution information to highlight possible identification problems at low resolving power that are caused by coincidences of lines and features. The spectra are available in electronic form from the authors.

**Key words:** Infrared: ISM: continuum – Infrared: ISM: lines and bands – Galaxies: individual: M 82 – Galaxies: individual: NGC 253 – Galaxies: individual: Circinus – Galaxies: individual: NGC 1068

## 1. Introduction

Mid-infrared spectra of galaxies are rich in emission lines, and display prominent broader emission and absorption features due to the presence of various solids and/or large molecules in their interstellar medium (ISM). Significant variation from source to source suggests that these features may provide important diagnostics of the ISM conditions in galaxies.

The ground based and Kuiper Airborne Observatory spectra of the prototypical starburst M 82 by Gillett et al. (1975) and Willner et al. (1977) fully established the existence of the mid-infrared ‘unidentified infrared bands’ (UIB) at 6.2, 7.7, 8.6, and 11.3  $\mu\text{m}$  in galaxy spectra. These emission bands are characteristic of C-C and C-H bonds in aromatic molecules. In this paper we will refer to them as ‘PAH features’ according to one of the most popular interpretations of their carrier, polycyclic aromatic hydro-

Send offprint requests to: sturm@mpe.mpg.de

<sup>★</sup> Based on observations with ISO, an ESA project with instruments funded by ESA member states (especially the PI countries: France, Germany, the Netherlands and the United Kingdom) and with participation of ISAS and NASA.

carbon molecules<sup>1</sup>. These detections and related work using the IRAS LRS (Cohen & Volk 1989) form the basic pre-ISO knowledge of mid-infrared spectral features in galaxies.

Considerable work has also been done from the ground but has been limited to the features found in atmospheric windows, mainly silicate absorption and PAH feature emission in the N band (e.g. Roche et al. 1991, and references therein) and the companion PAH feature in the L band (e.g. Moorwood 1986). The restriction to atmospheric windows increases problems in establishing the ‘continuum’ on which the features are superposed. This is a nontrivial task, even with full wavelength coverage, due to the crowding of mid-infrared emission and absorption features (especially in the  $10\mu\text{m}$  region).

With the Short Wavelength Spectrometer SWS (de Graauw et al. 1996) on board the Infrared Space Observatory ISO (Kessler et al. 1996) high spectral resolution observations with good signal-to-noise (S/N) were obtained for a number of bright galaxies. Their main advantages lie in continuous wavelength coverage from 2.4 to  $45\mu\text{m}$  and in the possibility to clearly separate features from nearby emission lines.

The interpretation of galaxy-integrated spectra strongly benefits from comparisons to similar observations of galactic sources, sometimes spatially resolved, allowing better isolation of the physical mechanisms at work. Recent ISO spectra of many galactic template objects, such as reflection nebulae (e.g. Boulanger et al. 1996, Cesarsky et al. 1996a, Verstraete et al. 1996, Moutou et al. 1998), planetary nebulae and circumstellar regions (e.g. Beintema et al. 1996), and HII regions (Roelfsema et al. 1996, Cesarsky et al. 1996b) have clearly demonstrated the importance of such template spectra. They prove that PAHs are an ubiquitous part of the ISM. Additional information on emission features of crystalline silicates comes from similar template observations with ISO of e.g. planetary nebulae (Waters et al. 1998), evolved stars (Waters et al. 1996), young stars (Waelkens et al. 1996), or LBGs in the LMC (Voors et al. 1999). Absorption features (silicates, ices) have been found e.g. in the Galactic center (Lutz et al. 1996, Chiar et al. 2000), young stellar objects (d’Hendecourt et al. 1996, Whittet et al. 1996, Dartois et al. 1999), and in dark clouds in the solar neighborhood (Whittet et al. 1998).

In this paper we present an inventory of mid-infrared spectral features detected in high resolution ( $R \sim 1500$ ) ISO-SWS 2.4– $45\mu\text{m}$  spectra of the starburst galaxies M82 and NGC 253, the Seyfert 2 galaxies Circinus and NGC 1068, and a position in the 30 Doradus star forming region of the Large Magellanic Cloud (Sect. 3). We

briefly discuss possible feature identifications (Sect. 4.1) and highlight possible relations between these features and the physical state of the interstellar medium in galaxies (Sect. 4.2). We also address the issue of the continuum determination and the apparent depth of the silicate absorption at  $9.7\mu\text{m}$  (Sect. 5). Finally (Sects. 6 and 7) we demonstrate the use of these ISO spectra as templates for future infrared missions such as SIRTf, with particular emphasis on potential identification problems at low resolving power that are caused by coincidences of lines and features.

All the spectra shown here exhibit a large number of atomic, ionic and molecular emission lines. These have been or will be discussed elsewhere, along with more details on observations and data processing (Circinus: Moorwood et al. 1996; M82: Lutz et al. 1998b, Schreiber 1998; NGC 1068: Lutz et al. 2000; 30 Dor: Thornley et al., in prep.).

## 2. Observations and data reduction

The objects discussed here have been observed as part of the ISO guaranteed time project on bright galactic nuclei. Here we concentrate on full grating scans obtained in SWS01 mode, speed 4. This mode provides a full 2.4– $45\mu\text{m}$  scan at resolving power of approximately 1000–2000. For NGC 253, Circinus, and NGC 1068 the observations were centered on the nuclei. In the case of M82 the observation was centered on the southwestern star formation lobe. For 30 Dor the apertures were lying roughly parallel to an ionized shell region, about  $0.5'$  away from the central stellar cluster. Table 1 summarizes the positions. Note that different parts of an SWS full grating scan are observed with different aperture sizes<sup>2</sup>, varying between  $14'' \times 20''$  and  $20'' \times 33''$ .

We have processed the data using the SWS Interactive Analysis (IA) system (Lahuis et al. 1998, Wieprecht et al. 1998) and the ISO Spectral Analysis Package ISAP (Sturm et al. 1998). Dark current subtraction, scan direction matching, and flatfielding have been done interactively, and noisy detectors have been eliminated. In ISAP we clipped outliers and averaged the data of all 12 detectors for each AOT band, retaining the instrumental resolution. For those wavelength ranges affected by fringes, the averaged spectra were defringed using the FFT or iterative sine fitting options of the defringe module within ISAP.

To reduce noise for display purposes (Fig. 1), we have smoothed the data with a gaussian filter to a uniform resolution of 1000. This broadens slightly the line widths of the narrow atomic and ionic emission lines, but does not affect the broad emission and absorption features discussed

<sup>1</sup> Other suggested carriers include small grains of hydrogenated amorphous carbon (HACs), quenched carbonaceous composites (QCCs), or coal.

<sup>2</sup> The aperture sizes are  $14'' \times 20''$  for 2.4– $12.0\mu\text{m}$ ,  $14'' \times 27''$  for  $12.0$ – $27.5\mu\text{m}$ ,  $20'' \times 27''$  for  $27.5$ – $29.0\mu\text{m}$ , and  $20'' \times 33''$  for  $29.0$ – $45\mu\text{m}$ , with some wavelength overlap between the bands.

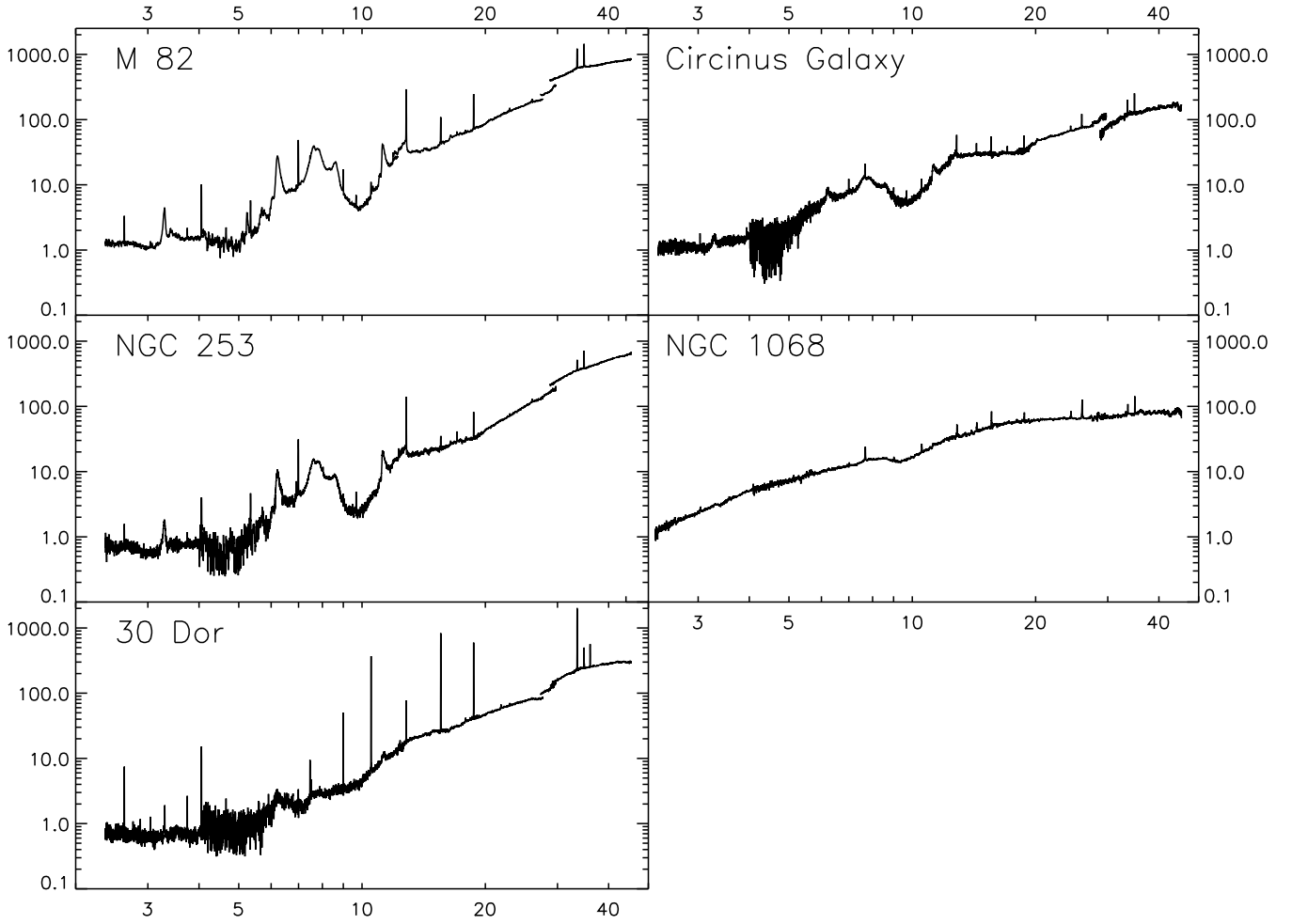


**Fig. 1.** The full SWS01 spectra of the five extragalactic templates. x-axis: wavelength in  $\mu\text{m}$ ; y-axis: flux density in Jansky.

**Table 1.** Summary of observed positions (J2000), and position angles.

| Object   | RA  | Decl.        | PA   | remark |
|----------|---|--------------|------|--------|
| M 82     | 09 <sup>h</sup> 55 <sup>m</sup> 50.7 <sup>s</sup> | 69°40′44.4″  | 245° | 1      |
| NGC 253  | 00 <sup>h</sup> 47 <sup>m</sup> 33.2 <sup>s</sup> | -25°17′17.2″ | 28°  | 2      |
| 30 Dor   | 05 <sup>h</sup> 38 <sup>m</sup> 46.0 <sup>s</sup> | -69°05′07.9″ | 230° | 3      |
| Circinus | 14 <sup>h</sup> 13 <sup>m</sup> 09.7 <sup>s</sup> | -65°20′21.5″ | 19°  | 2      |
| NGC 1068 | 02 <sup>h</sup> 42 <sup>m</sup> 40.8 <sup>s</sup> | -00°00′47.3″ | -11° | 2      |

1 = SW lobe  
 2 = nucleus  
 3 = ionized shell

in this paper. We did not remove the flux jumps at detector band limits. Part of these jumps may be real because the sources are extended and because the aperture sizes change at some band edges (at approximately 12.0, 27.5 and 29.0  $\mu\text{m}$ ). Another part simply reflects the flux calibration uncertainty, which is of the order of 20 per cent.

We carefully checked the reality of the features in the final spectra against the possibility of residual instrumental features from the Relative Spectral Response Function (RSRF), which might be caused e.g. by an improper dark current subtraction. For example, the detector RSRF exhibits absorption features at 11.05 and 34  $\mu\text{m}$  which might appear in emission in the calibrated spectrum. This is, however, at most an effect of the order of a few per cent of the continuum level. The features we see at these wavelengths in our spectra (see below) are stronger, so that they must be real. Furthermore, we checked whether a feature appears in both scan directions and in the majority of all detectors. Additional confirmation was possible for those features that lie in the overlap region of two different AOT bands and appear in both bands. At this stage of instrument calibration, we do not believe that any of the broad structures in band 3E (appr. 27.5–29.5  $\mu\text{m}$ ) are real features. Also, features at the end of band 4 (43–45  $\mu\text{m}$ , e.g. in Circinus) cannot be trusted.

**Table 2.** Summary of observed broad emission features (approximate peak positions in  $\mu\text{m}$ ). Uncertain detections are given in parentheses, nondetections are marked by a dash.

| M 82   | NGC 253 | 30 Dor | Circinus | NGC 1068 | nearby lines                                   |
|--------|---------|--------|----------|----------|--|
| 3.25   | 3.25    | —      | 3.25     | —        |  |
| 3.3    | 3.3     | 3.3    | 3.3      | 3.3      | Pf <sub><math>\delta</math></sub>              |
| 3.4    | 3.4     | 3.4    | —        | —        |  |
| 3.5    | (3.5)   | 3.5    | —        | —        |  |
| —      | 3.75    | —      | 3.75     | —        |  |
| 5.25   | —       | —      | —        | —        |  |
| 5.65   | 5.65    | —      | —        | —        |  |
| 6.0    | 6.0     | 6.0    | (6.0)    | —        |  |
| 6.2    | 6.2     | 6.2    | 6.2      | (6.2)    |  |
| 6.3    | 6.3     | 6.3    | 6.3      | —        |  |
| 7.0    | 7.0     | (7.0)  | —        | —        | H <sub>2</sub> +<br>[Ar II]                    |
| 7.6    | 7.6     | 7.6    | 7.6      | (7.6)    | Pf <sub><math>\alpha</math></sub> +<br>[Ne VI] |
| 7.8    | 7.8     | 7.8    | 7.8      | 7.8      |  |
| 8.3    | —       | —      | —        | —        |  |
| 8.6    | 8.6     | 8.6    | 8.6      | 8.6      |  |
| (10.6) | —       | —      | —        | —        | [S IV]   |
| 11.05  | 11.05   | 11.05  | 11.05    | 11.05    |  |
| 11.25  | 11.2    | 11.25  | 11.25    | 11.25    |  |
| 12.0   | 12.0    | 12.0   | —        | —        |  |
| 12.7   | 12.7    | —      | 12.7     | (12.7)   | [Ne II]  |
| 13.55  | 13.55   | (13.5) | 13.6     | 13.4     |  |
| 14.25  | 14.25   | 14.25  | 14.25    | —        | [Ne V]+<br>[Cl II]                             |
| (14.8) | (14.8)  | (14.8) | (14.8)   | —        |  |
| 15.7   | 15.7    | 15.7   | 15.85    | 15.9     | [Ne III]                                       |
| 16.5   | 16.5    | 16.5   | —        | —        |  |
| (17.4) | (17.4)  | —      | —        | —        |  |
| (18.0) | —       | (18.0) | —        | —        |  |
| 20.5   | (20.3)  | (20.4) | 20.2     | —        |  |
| —      | —       | —      | 21.7     | —        |  |
| 34     | 34      | 34     | 34       | —        | [Si II]+<br>[S III]                            |

### 3. An inventory of features

In Tables 2 and 3 we give an inventory of features that we believe to be reliable detections. We consider a detection reliable if the feature has an amplitude of at least  $3\sigma$  of the noise level and if it fulfills the criteria described above. We also list a few uncertain detections in parentheses, e.g. features in compliance with the above criteria but with an amplitude of less than  $3\sigma$  (but note that the definition of the local noise level is in many cases somewhat uncertain). Most of these features have been described before in reports of ISO-SWS observations of galactic template sources (e.g. Moutou et al. 1996, Verstraete et al. 1996, Roelfsema et al. 1996, Beintema et al. 1996). Here we highlight a few of their characteristics, source by source. In

**Table 3.** Summary of observed absorption features. Uncertain detections are given in parentheses.

| M 82           | NGC 253        | 30 Dor         | Circinus       | NGC 1068 | species              |
|----------------|----------------|----------------|----------------|----------|----------------------|
| 3.0            | 3.0            | —              | —              | —        | H <sub>2</sub> O ice |
| — <sup>1</sup> | — <sup>1</sup> | — <sup>1</sup> | — <sup>1</sup> | 3.4      | hydrocarbon          |
| (9.7)          | (9.7)          | —              | (9.7)          | 9.4      | silicate             |
| (18.0)         | (18.0)         | —              | (18.0)         | —        | silicate             |

<sup>1</sup> could be filled in by PAH emission

**Table 4.** Approximate absolute and relative fluxes of the prominent PAHs at 3.3 and 6.2  $\mu\text{m}$  (see text for details).

| Object   | flux <sup>1</sup> | 3.3 $\mu\text{m}$<br>relative flux <sup>2</sup> | flux <sup>1</sup> | 6.2 $\mu\text{m}$<br>relative flux <sup>2</sup> |
|----------|-------------------|---|-------------------|---|
| M 82     | 3.3               | 0.2   | 37                | 2.7   |
| NGC 253  | 1.0               | 0.1   | 13                | 1.7   |
| 30 Dor   | 0.3               | 0.04  | 1.5               | 0.2   |
| Circinus | 0.7               | 0.06  | 6.3               | 0.6   |
| NGC 1068 | 0.3               | 0.02  | 1.0               | 0.05  |

<sup>1</sup> [ $10^{-18}$  W/cm<sup>2</sup>]

<sup>2</sup> PAH flux/continuum(11.6–11.9  $\mu\text{m}$ )

**Table 5.** Approximate absolute and relative fluxes of the prominent PAHs at 7.7 and 11.3  $\mu\text{m}$  (see text for details).

| Object   | flux <sup>1</sup> | 7.6–7.8 $\mu\text{m}$<br>relative flux <sup>2</sup> | flux <sup>1</sup> | 11.3 $\mu\text{m}$<br>relative flux <sup>2</sup> |
|----------|-------------------|---|-------------------|--|
| M 82     | 99                | 7.2   | 16                | 1.2  |
| NGC 253  | 39                | 5.0   | 7.2               | 0.9  |
| 30 Dor   | 0.3               | 0.04  | 1.7               | 0.2  |
| Circinus | 21                | 1.9   | 3.9               | 0.4  |
| NGC 1068 | 2.1               | 0.1   | 1.1               | 0.06   |

<sup>1</sup> [ $10^{-18}$  W/cm<sup>2</sup>]

<sup>2</sup> PAH flux/continuum(11.6–11.9  $\mu\text{m}$ )

Sect. 4.1 we briefly discuss possible identifications. Please note that many of the features are severely blended and thus the peak wavelengths given here are approximate.

We also list the fluxes of four of the most prominent PAHs in Tables 4 and 5. To measure these fluxes we defined continua by a linear interpolation between the following points: 2.50 and 3.65  $\mu\text{m}$  for the 3.3  $\mu\text{m}$  feature, 5.9 and 10.9  $\mu\text{m}$  for the features at 6.2 and 7.7  $\mu\text{m}$ , and 10.9 and 11.8  $\mu\text{m}$  for the 11.3  $\mu\text{m}$  feature. We then obtained the fluxes by integrating between the following band limits: 3.10–3.35  $\mu\text{m}$ , 6.0–6.5  $\mu\text{m}$ , 7.3–8.2  $\mu\text{m}$ , and 11.1–11.7  $\mu\text{m}$ . To give an indication of the relative contribution of these features to the infrared luminosity we also list their ratio to the continuum flux in the range 11.6–11.9  $\mu\text{m}$ . Due to the

uncertainties involved in this measuring process (continuum shape, feature profile, etc.) all absolute and relative fluxes are only approximate. By definition, these fluxes ignore a possible, PAH-related ‘plateau’ or ‘continuum’ in the 6–9 and 10–13  $\mu\text{m}$  range (e.g. Boulanger et al. 1996).

**M 82:** M 82 is a small galaxy undergoing a very powerful starburst, and is considered to be a prototype of starburst activity. Due to its proximity (3.63 Mpc, Freedman et al. 1994) it is the brightest galaxy in the infrared, with the infrared luminosity arising mainly from warm dust in the central region. Emission features at 8.7 and 11.3  $\mu\text{m}$  were first detected by Gillett et al (1975), and the 3.3, 6.2 and 7.6  $\mu\text{m}$  features by Willner et al. (1977).

The main PAH features are clearly seen in the mid-infrared spectrum of M 82, shown in its entirety in Fig. 1 and in detail in the top panels of Fig 2. In addition, the spectrum shows a large number of weaker features which have previously been detected with ISO only in galactic template sources.

The 3.3  $\mu\text{m}$  feature has satellites at 3.4 and 3.5  $\mu\text{m}$ . It also shows a blue asymmetry, which might be due to a feature at 3.25  $\mu\text{m}$  (see Beintema et al. 1996). Two weak features at 5.25 and 5.65  $\mu\text{m}$ , that have been observed e.g. in the planetary nebula NGC 7027 (Beintema et al. 1996) and the photodissociation front of M 17 (Verstraete et al. 1996), are also present in M 82. The 6.2  $\mu\text{m}$  band has a red shoulder and shows an additional feature at 6.0  $\mu\text{m}$ . The 7.7  $\mu\text{m}$  feature consists of two bands at 7.6 and 7.8  $\mu\text{m}$ . A significant contribution of 7.7  $\mu\text{m}$  solid methane absorption (e.g. Whittet et al. 1996, Lutz et al. 1996) to this strong dip between 7.6 and 7.8  $\mu\text{m}$  is unlikely, since in M 82 related icy absorption features are shallower and extinction is lower (Sect. 5) than in the sources with clear methane absorptions. A weak feature is present at 10.6  $\mu\text{m}$ , which is confirmed in the average starburst spectrum of Lutz et al. 1998a (their Fig. 1, independent ISOPHOT-S data), and probably related to a feature seen by Beintema et al. (1996) in the spectrum of NGC 7027. The 11.3  $\mu\text{m}$  feature peaks at 11.2  $\mu\text{m}$  and shows the well-known asymmetric shape towards longer wavelengths (Witteborn et al. 1989). There is an additional component around 11.05  $\mu\text{m}$ , much too strong to be related to artifacts from the RSRF correction known to exist at this wavelength. A weak feature may be present near 12.0  $\mu\text{m}$ . The 12.7  $\mu\text{m}$  feature is very prominent in M 82. Moutou et al. (1998) found two emission features at 15.8 and 16.4  $\mu\text{m}$  in the spectrum of the galactic reflection nebula NGC 7023. On the basis of their laboratory work, they attributed these features to PAH molecules. These two features are clearly seen in M 82, and in some of our other template spectra. More emission features can be found at still longer wavelengths (20.5 and 33–34  $\mu\text{m}$ ).

In addition we find two features that – to our knowledge – have not been reported before: at 7.0 and 8.3  $\mu\text{m}$ . A feature around 7.0  $\mu\text{m}$  is also present in NGC 253 (most

clearly), and perhaps in 30 Dor. We found the same feature in ISO-SWS spectra of the cool, dusty envelopes of the planetary nebula He 2-113 (see e.g. Waters et al. 1998, their Fig. 2). The average ISOPHOT-S spectra of starburst and normal galaxies (Lutz et al. 1998a, Helou et al. 2000) also show hints of a weak feature, blended with H<sub>2</sub> S(5) 6.91  $\mu\text{m}$  and [Ar II] 6.99  $\mu\text{m}$  (see also Sect. 6). The 8.3 feature is also visible in the galactic template spectrum of NGC 7023 (Fig. 4), and perhaps in some of the compact HII regions shown in Roelfsema et al. (1996). We also want to mention here the 14.3  $\mu\text{m}$  band. An astronomical observation of this band has been reported only recently for the first time (Tielens et al. 1999). It is present in all our template spectra, with the exception of NGC 1068, in NGC 7023, and perhaps also in some of the circumstellar PAH spectra shown in Beintema et al. (1996). On the other hand, our spectra do not show some of the emission features that have been detected before in astronomical observations, e.g. at 4.65  $\mu\text{m}$  (Verstraete et al. 1996) and 13.3  $\mu\text{m}$  (Moutou et al. 1998).

There are very few absorption features in our spectrum of M 82. The trough around 10  $\mu\text{m}$  looks like a strong 9.7  $\mu\text{m}$  silicate feature. In Sect. 5 we argue, however, that the trough is mainly due to the strong PAH emission at 8.7 and 11.3  $\mu\text{m}$ . Also, there is no clear signature of a corresponding silicate absorption feature at 18  $\mu\text{m}$ . A broad absorption feature around 3.0  $\mu\text{m}$  is probably due to H<sub>2</sub>O-ice. Its optical depth ( $\tau \sim 0.2$ ) is relatively small compared e.g. to the Galactic center ( $\tau = 0.5$ , Lutz et al. 1996, Chiar et al. 2000). However, since the overall extinction estimates differ in the same sense, this is consistent with the M 82 line of sight having properties similar to that towards the Galactic center: a mixture of diffuse ISM and molecular cloud extinction, with some variance in the relative weight for different lines of sight (Chiar et al. 2000). These properties seem to be quite typical for starburst galaxies, as we find similar conditions in NGC 253 (see below) and in NGC 4945 (Spoon et al., in prep.).

The M 82 spectrum has the highest S/N ratio and shows the largest number of features in our sample. Combined with the ISO-LWS long wavelength spectrum (Colbert et al. 1999) it will be an important template for future missions.

**NGC 253:** NGC 253 is a nearby, almost edge-on barred spiral galaxy with a high level of circumnuclear starburst activity. At optical wavelengths the galaxy is heavily obscured by dust lanes in the central regions. The ionic emission lines in NGC 253 are of lower excitation (e.g. lower [Ne III]/[Ne II] ratio) than in M 82, suggesting a softer average radiation field (Thornley et al., in prep.). Despite these differences between the two galaxies, their spectra of broad emission features are remarkably similar. This is demonstrated in Fig. 3. Only beyond 9  $\mu\text{m}$  does a difference in the underlying continuum become obvious. NGC 253 has a stronger continuum at these longer wave-

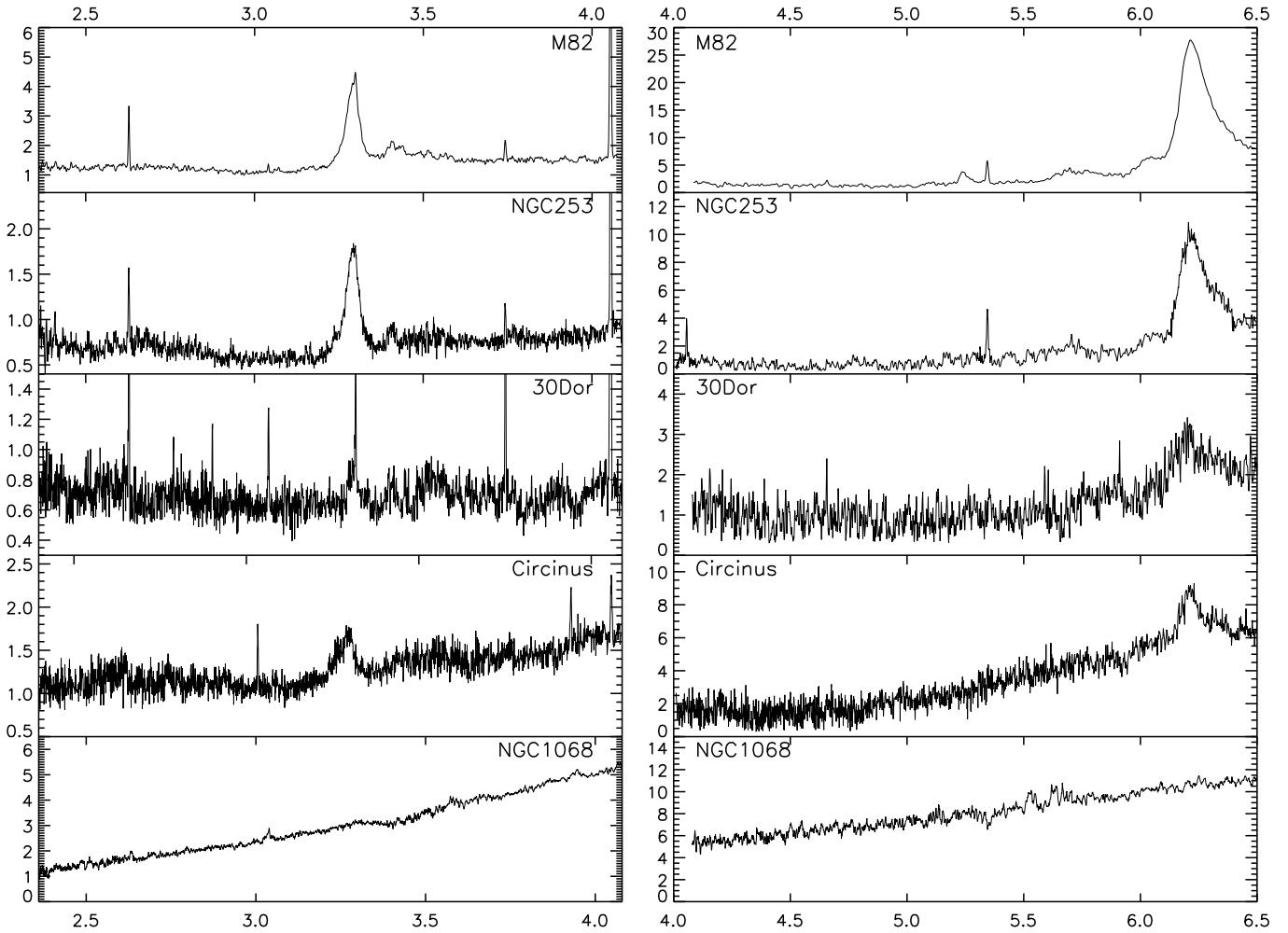


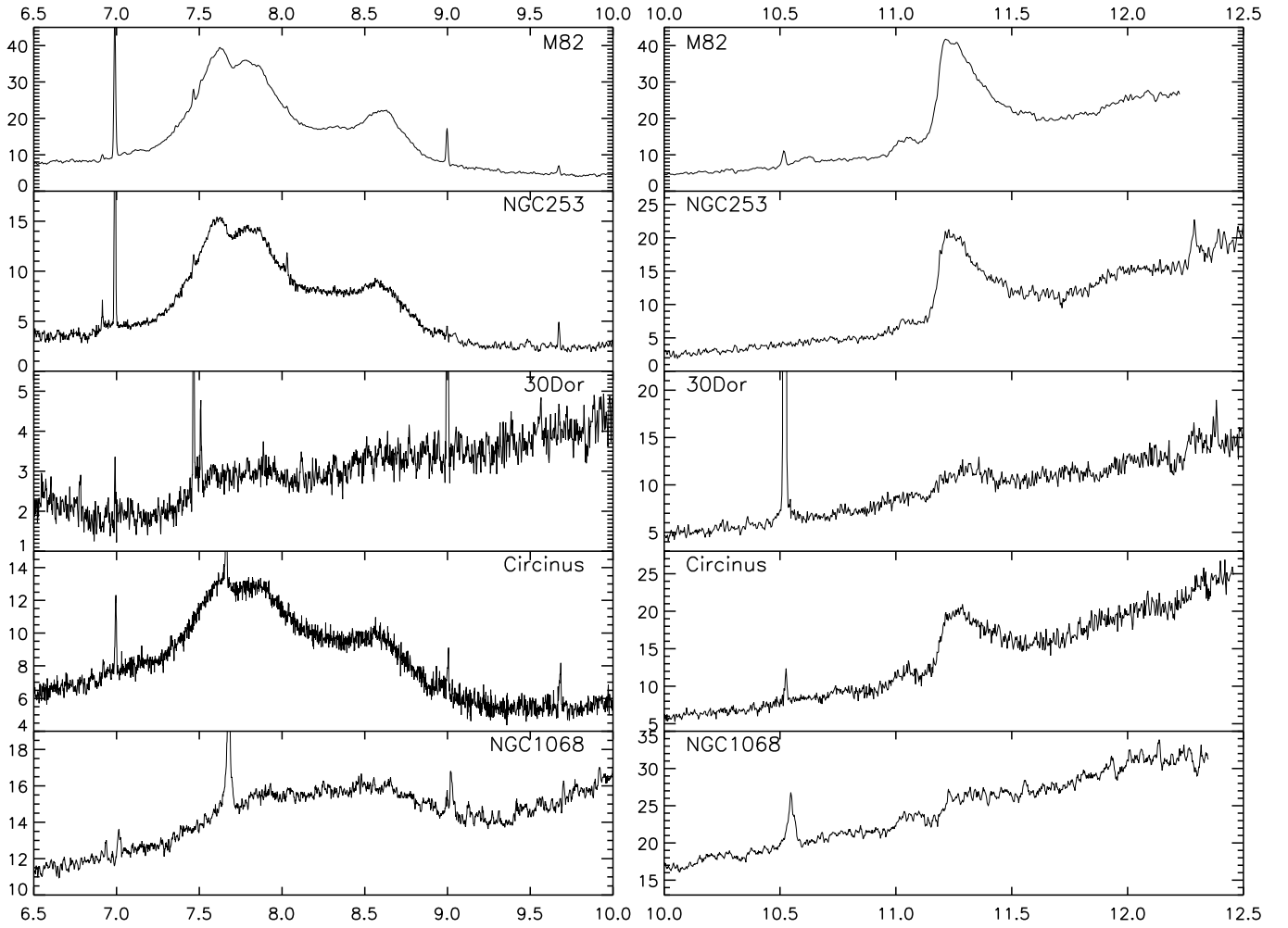
**Fig. 2.** Details of the spectra. Wavelength in  $\mu\text{m}$ , flux density in Jansky.

lengths. In starburst galaxies this underlying continuum is usually attributed to very small grains (VSG) of dust (e.g. Désert et al. 1990). In Sect. 5 we will use the difference in the continua of M82 and NGC 253 to characterise the shape of the VSG continuum.

Table 2 shows that nearly all features of M82 are also seen in NGC 253. The very few exceptions may simply be due to the lower S/N ratio of the NGC 253 spectrum. The red shoulder of the  $6.2\mu\text{m}$  band seen in M82 is more prominent in NGC 253 and is probably due to an additional feature at  $6.35\mu\text{m}$ . The  $3.0\mu\text{m}$  ice absorption is also present, having an optical depth of  $\tau \sim 0.25$ .

**30 Dor:** The 30 Dor region in the LMC is the largest, most massive, and most luminous H II region in the Local Group. As a local template for massive star formation and its interaction with the interstellar medium, it is instructive to compare its spectrum to the galaxy spectra in our sample. A more detailed study of the mid-infrared fine structure emission lines in 30 Dor will be presented in an upcoming paper (Thornley et al., in prep.).

An inspection of Fig. 2 and Table 2 shows that the 30 Dor spectrum exhibits most of the PAH features found in the galaxy spectra. Lower S/N may contribute to the non-detection of some of the weak features. Compared to the two starburst galaxies, the features in 30 Dor are much weaker relative to the continuum (see also Tables 4 and 5) and show different ratios. Note, for instance, the high  $6.2/7.7\mu\text{m}$  feature ratio, the unusually high  $3.4/3.3$  ratio ( $\approx 0.5$ , see also Sect. 4.2), the shape of the  $7.6/7.8\mu\text{m}$  features, or the complete absence of the  $12.7\mu\text{m}$  feature. These differences may be partly due to the fact, that the SWS apertures covered only part of the entire 30 Dor complex. Verstraete et al. (1996) use the case of M17 to demonstrate the strong variations in PAH spectra going from the center of an H II region to the surrounding photodissociation region. On the other hand, the similarity of the 30 Dor spectrum to the integrated ISOPHOT-S spectrum of the dwarf galaxy NGC 5253 (Rigopoulou et al. 1999) strongly suggests that the weakness of the PAHs is not an aperture effect but reflecting an intrinsic property

Fig. 2. *continued*

of very active star formation in a low metallicity environment.

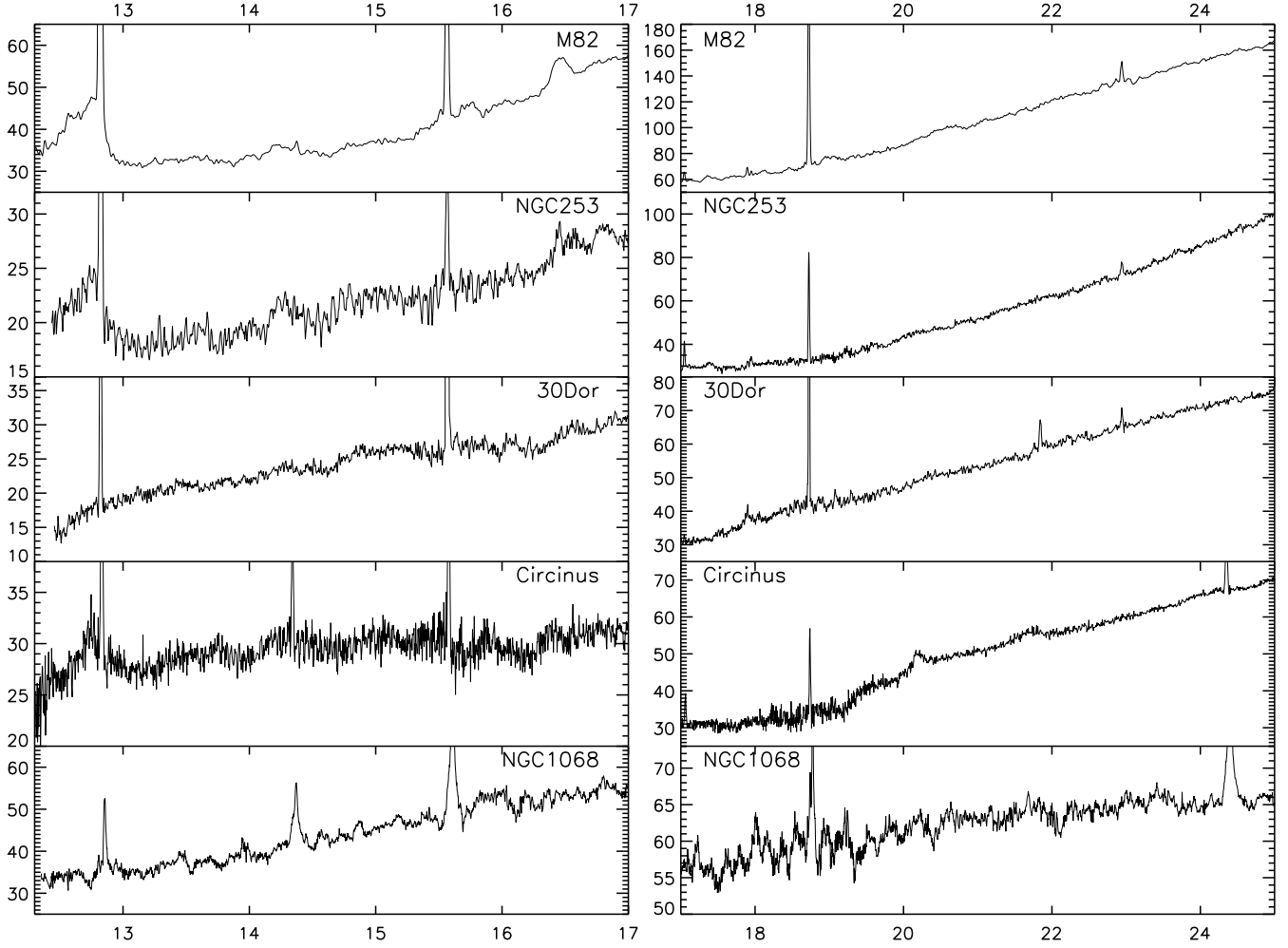
Silicate absorption at  $9.7$  and  $18\mu\text{m}$  is, if at all present, very weak. No other absorption features can be detected.

**NGC 1068:** The nearby, prototypical Seyfert 2 galaxy NGC 1068 is a key object in the investigation and modeling of active galactic nuclei (AGNs). The ISO-SWS observations were centered on the active nucleus, with the aperture covering very little of the circumnuclear star forming ‘ring’, which has a radius of  $\approx 15''$ . In stark contrast to the starburst templates we have shown, this active nucleus spectrum shows very little PAH emission. The weaker features (e.g.  $3.3$ ,  $6.2$  or  $12.7\mu\text{m}$ ) are barely visible, if at all.

The continuum around  $10\mu\text{m}$  is strong because of a central warm component heated by the AGN. Silicate absorption is clearly present, although centered at  $9.4\mu\text{m}$  rather than at  $9.7\mu\text{m}$ , but again surrounding weak PAH emission complicates its interpretation. Hydrocarbon absorption is seen at  $3.4\mu\text{m}$  (see also Bridger et al. 1994), in contrast to our starburst templates, where it is not

observed. Note, however, that in M82 and NGC 253 a similar absorption feature could plausibly exist if the analogy to the Galactic center holds, but be filled in by the  $3.3/3.4$  PAH emission. On the other hand M82 and NGC 253 show an  $\text{H}_2\text{O}$  ice absorption at  $3.0\mu\text{m}$  which is definitely absent in NGC 1068. These differences in absorption features are entirely plausible because of the different physical conditions in the obscuring regions. For the starbursts, they likely include diffuse ISM as well as molecular clouds that can host icy grains. Conversely, infrared polarimetry suggests that most of the near-infrared obscuration in NGC 1068 occurs within a few parsecs from the nucleus, possibly in the torus (e.g. Packham et al. 1997). Such an energetic environment will be much less favourable for the existence of icy grains.

**Circinus:** The Circinus Galaxy is a nearby spiral galaxy which shows Seyfert 2 activity (e.g. Moorwood & Glass 1984, Oliva et al. 1994, Moorwood et al. 1996, Oliva et al. 1998). Due to its proximity (5 times closer than NGC 1068) it has become another template object for the

Fig. 2. *continued*

study of AGNs. The AGN is surrounded by circumnuclear star-forming regions, as is often the case in Seyfert nuclei residing in spirals. The ISO-SWS observations were centered on the active nucleus, but contrary to the observations of NGC 1068 the apertures covered a significant amount of this circumnuclear star formation. Hence, most of the dust emission features seen in the starburst templates are also found in Circinus, but with weaker line-to-continuum ratio (see the discussion in Sect. 4.2). A peculiarity of the Circinus spectrum are the very pronounced features in the 20–22  $\mu\text{m}$  region.

The observation was performed very early in the mission, when the observing strategy was not yet fully optimized. For instance, exposures of the internal flux calibration lamps, preceding observations of the scientific target, caused memory effects in the immediately following scans. The low flux level of band 4 ( $\lambda \geq 29 \mu\text{m}$ ), relative to the preceding bands, is due to such a memory effect and an incorrect dark current subtraction. The same might be true for the apparent features near 44  $\mu\text{m}$  (which are not visible in the overlapping LWS spectrum). We did not attempt

to improve the dark current subtraction further since this would involve subjective assumptions about the true dark current.

#### 4. Mid-infrared features and the physical state of the ISM

##### 4.1. Identification

##### 4.1.1. The 2–13 $\mu\text{m}$ region:

The emission features in this wavelength range have been extensively studied with ISO in galactic objects during the last few years. Comprehensive discussions of their identifications and characteristics can be found e.g. in Beintema et al. (1996), Moutou et al. (1998), Roelfsema et al. (1996), and Verstraete et al. (1996). They are most often attributed to PAH molecules. This is supported by recent laboratory studies (e.g. Roelfsema et al. 1996, Moutou et al. 1996). The only features in this range, which have not been addressed in the literature so far, are the ones at 7.0 and 8.3  $\mu\text{m}$ . In our sample of galaxies they are unam-



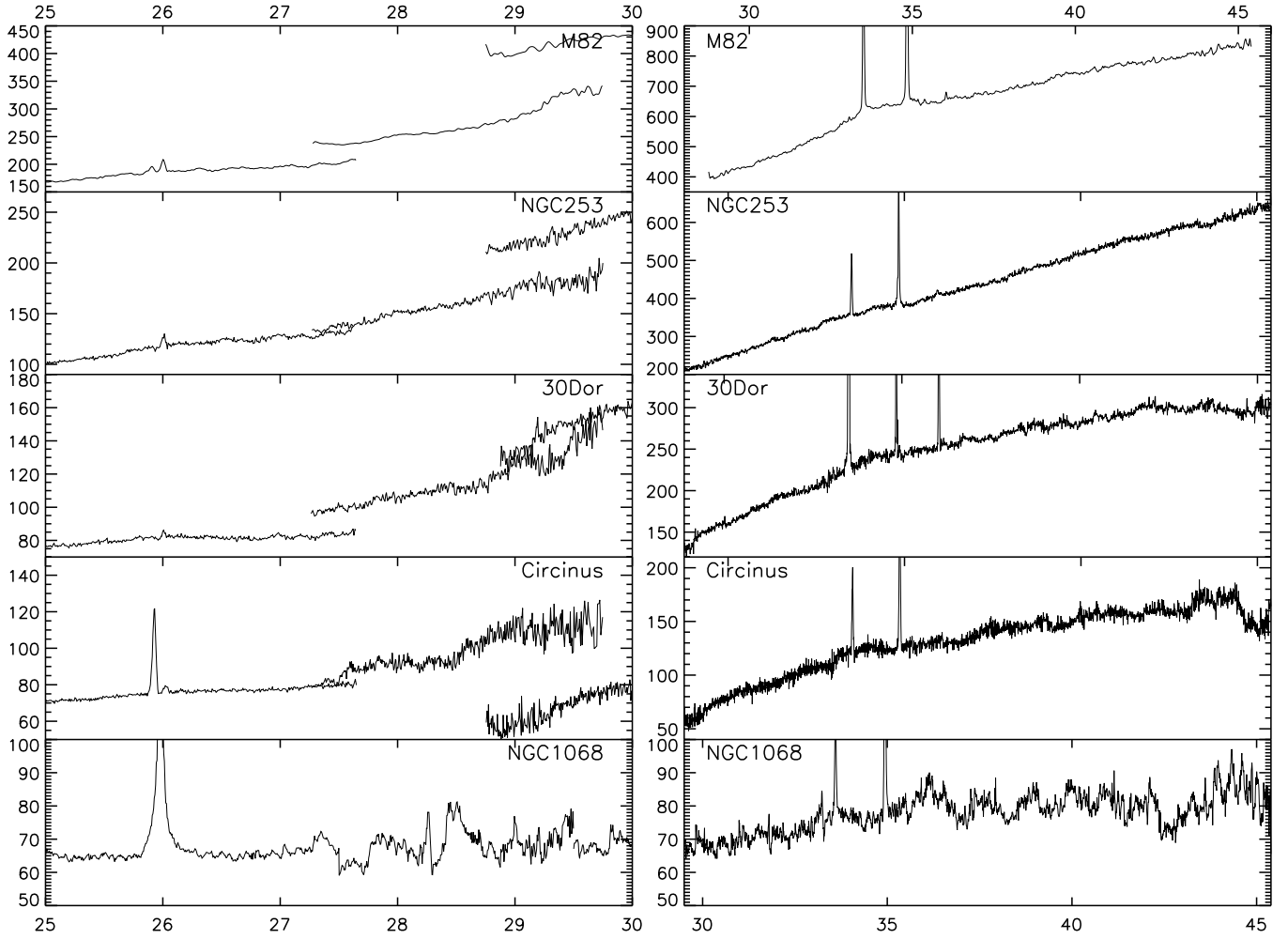


**Fig. 2.** *continued.* Broad features between 27.5 and 29.5  $\mu\text{m}$ , and longward of 40  $\mu\text{m}$  cannot be trusted.

biguously detected only in M 82 and NGC 253 (the 8.3  $\mu\text{m}$  feature only in M 82), but as mentioned in Sect. 3 they seem to be present in other published spectra as well. It seems likely that they can be attributed to a PAH modes, too.

#### 4.1.2. Features between 13 and 20 $\mu\text{m}$ :

Features in this range have attracted less attention in the past, because they are intrinsically weak (but see e.g. Beintema et al. 1996). These bands, however, are more sensitive to the molecular structure of PAHs, since they involve the motion of the molecule as a whole, therefore depending on the exact species (Léger et al. 1989). Hence, their observation could help to better constrain the composition of the interstellar mixture. The 13.6, 15.8, and 16.5  $\mu\text{m}$  features are also visible in the spectra of NGC 7023 and have been attributed to PAH bands in the past by Moutou et al. (1998), based on their laboratory work. The band at 14.3  $\mu\text{m}$  has been tentatively attributed to a phenyl bending mode by Tielens et al. (1999). Moutou et al. (1996) list

a feature at this wavelength in their composite laboratory spectrum of a mixture of PAHs. Although weak, it might cause confusion with [Ne V] in low resolution spectra (see Sect. 6). Finally, the weak feature at 14.8  $\mu\text{m}$  (if real) could be due to the smallest PAH, benzene (Tielens et al. 1999).

#### 4.1.3. Features in the 20 to 45 $\mu\text{m}$ region:

The number of modes in the laboratory PAH spectra of Moutou et al. (1996) decreases with increasing wavelength. Few species show emission beyond 20  $\mu\text{m}$ , e.g. near 21, 28 and 40  $\mu\text{m}$ . In this wavelength range other sources must be taken into account. A number of recent papers have reported the detection of crystalline silicates (olivines, forsterite, pyroxene, etc.) in objects like Luminous Blue Variables (Voors et al. 1999), dusty circumstellar disks (Waelkens et al. 1996, Waters et al. 1996), or Planetary Nebulae (Waters et al. 1998). In particular the feature at 34  $\mu\text{m}$  could be attributed to these kind of sources. However, one would expect to see emission features at e.g. 23, 28, 40 and 43  $\mu\text{m}$ , as well; none of these

features are clearly detected in our spectra. On the other hand, even in some of the galactic templates, such as the planetary nebula NGC 6543 (e.g. Waters et al. 1996), not all of these features are present.

A feature near  $20.5\mu\text{m}$  shows a striking variation in shape and central wavelength between the galaxies. This is particularly surprising since the galaxy spectra include a mixture of many different regions, and may suggest a carrier occurring only transiently in very special conditions. In Circinus this feature is most prominent, and peaks at the bluest wavelength ( $20.2\mu\text{m}$ ). Circinus also shows a second peak at  $21.7\mu\text{m}$  which is absent in the other spectra. A bump around  $20.5\mu\text{m}$  is also seen in ISO-SWS spectra of M supergiants (Voors et al. 1999, Molster et al. 1999). It could be due to PAHs or alternatively metal oxides like FeO (Waters et al. 1996, Henning et al. 1995). IRAS-LRS and ISO-SWS spectroscopy have also detected a broad feature, centered at approximately  $20.1\mu\text{m}$ , in carbon rich stars (Volk et al. 1999, García-Lario et al. 1999, Szczerba et al. 1999). Possible candidates that have been proposed include large PAH clusters or hydrogenated amorphous carbon grains, hydrogenated fullerenes, and nano-diamonds (see references in Volk et al. 1999). However, compared to these detections, the features in our spectra are much narrower.

A mixture of fullerene molecules of different degree of hydrogenation (Webster 1995) might also explain the second peak in Circinus around  $21.7\mu\text{m}$ , since the emission peak shifts from 23 for fully hydrogenated fullerene ( $\text{C}_{60}\text{H}_{60}$ ) to  $19\mu\text{m}$  for non-hydrogenated fullerene ( $\text{C}_{60}$ ). None of the other galaxies exhibit this feature, but the SWS01 spectrum of NML Cyg (Voors et al. 1999) and of the galaxy NGC 4945 (S. Lord, private communication) also show a weak emission feature around  $21.6\text{--}22\mu\text{m}$ .

The broad plateau at  $33\text{--}34\mu\text{m}$ , i.e. under the strong lines of [Si II] and [S III], could be affected by detector memory effects. To remove such a possible instrumental effect we treated the two different scan directions of the SWS01 mode separately. The trailing wings of each line profile, i.e. the blue wing for the scan with increasing wavelength, and the red wing for the scan decreasing in wavelength, are much more distorted by memory effects than the leading wings. Therefore, we cut out these trailing wings, before we averaged the spectra of the two scan directions. We are hence confident that most of the remaining plateau is real. Such a feature has been observed in many galactic targets and is generally attributed to crystalline silicates (olivine, e.g. Waters et al. 1998).

#### 4.2. Variation of PAH features

Published mid-IR spectra of galactic template sources show a significant variation of intrinsic PAH ratios from source to source. For instance Roelfsema et al. (1996) see a drastic change in the relative intensities of the 7.7 and 8.6 bands with increasing intensity or hardness of the radia-

tion field. Similar changes are seen e.g. in different regions of M17 (Verstraete et al. 1996) or - for the 8.6/11.3 ratio - in the reflection nebula NGC 1333 (Joblin et al. 1996). PAHs exposed to intense and hard radiation fields can be ionized, lose hydrogen atoms, or be photodissociated; any of these effects may contribute to the observed variations in PAH ratios. According to Joblin et al. (1996) the ionization is best traced by the 3.4/3.3 and 8.6/11.3 ratios. A good hydrogenation indicator is the  $(12+12.7)/11.3$  ratio. For instance, these authors find a high 3.4/3.3 ratio of 0.1 in radiation fields that are  $10^5$  times the standard.

Another important factor that can alter observed PAH ratios is extinction. Extinction will suppress the 6.2, 8.6 and  $11.3\mu\text{m}$  features with respect to the one at  $7.7\mu\text{m}$ . The 12.7/11.3 ratio is similarly affected, since the 11.3 feature is still in the wing of the  $9.7\mu\text{m}$  silicate absorption. Details will depend on the applicable extinction law (see e.g. the Galactic center, Lutz et al. 1996). While extinction clearly affects PAH spectra in highly obscured sources like Ultraluminous Infrared Galaxies (ULIRGs, Lutz et al. 1998a) or the edge-on galaxy NGC 4945 (Spoon et al., in prep.), its effect will be less pronounced in the lower extinction sources of our sample.

Finally, in active galaxies, such as NGC 1068 or the Circinus Galaxy, PAH features can be diluted by an AGN-powered hot dust continuum. Genzel et al. (1998) and Lutz et al. (1998a) have used this as a diagnostic of the power sources of ULIRGs.

Our sample of galaxy spectra exhibits a similar trend in relative PAH strengths as the galactic templates. M 82 and NGC 253 have high 3.4/3.3 ratios, consistent with them being active starburst galaxies. 30 Dor seems to have an even higher 3.4/3.3 ratio, but the S/N ratio is not sufficient for a detailed analysis. However, a strong and hard, highly ionizing radiation field in 30 Dor is consistent with the results of Thornley et al. (1998), which are based on the ratios of fine structure emission lines, like [Ne III]/[Ne II]. In that context it is interesting to note again the complete absence of the  $12.7\mu\text{m}$  feature in 30 Dor. In the two starburst galaxies M 82 and NGC 253 we see well-separated 7.6/7.8 and 8.6 features. The 8.6 band is much weaker than the 7.6/7.8 band, just as observed in ‘normal’ HII regions. In the Seyfert galaxy NGC 1068, however, the 8.6 band is similar in strength to the 7.7 band, as it is seen in the ultracompact HII regions in M 17 (Cesarsky 1996b) or IRAS 18323-0242 (Roelfsema et al. 1996), where the UV radiation field is extremely strong.

NGC 1068, like many AGNs, shows an additional component of warm dust in the  $10\mu\text{m}$  region. Unified models for Seyfert galaxies predict a dusty torus which would emit at these mid-infrared wavelengths (e.g. Pier & Krolik 1992). Hence, an alternative interpretation of the weak emission features on both sides of the silicate absorption might be self-absorbed silicate emission from the torus, i.e. the emissions we identified as PAH might simply be wings of a wide silicate emission maximum, the center of which

is suppressed by absorption. However, the observed double peaks at 7.7/8.6 and 11.05/11.25, as well as the distinct rise in flux near  $7.3\mu\text{m}$  are not reproduced by torus models and show that there must be some real, although weak, PAH emission on top of the continuum. The weakness of the PAH emission can be understood in terms of dilution by the hot dust continuum and destruction by the intense AGN radiation field.

NGC 1068 has a circumnuclear starburst region, and some of the PAH emission might be picked up from this region by the large SWS aperture. The match in shape with the (small-aperture) ground-based data of Roche et al. (1984) in the 8–13 $\mu\text{m}$  range, and comparisons to ground-based CO maps, suggest that this effect is of minor importance here.

In the Circinus Galaxy the 7.7/8.6 ratio is somewhere in between the two extrema M82 and NGC 1068. The feature/continuum ratio of the PAH features, however, is much higher in Circinus than in NGC 1068. We attribute this to the fact that in the case of Circinus the large SWS aperture indeed picked up parts of the well-known circumnuclear star forming region.

## 5. Continuum placement and the depth of the silicate feature

An important diagnostic in many extragalactic studies is the depth of the silicate absorption feature at  $9.7\mu\text{m}$  and the extinction derived from it. However, the presence of strong PAH bands on both sides of the  $9.7\mu\text{m}$  silicate feature makes it very difficult to estimate the continuum level and the true depth of the silicate absorption. In particular ground-based 8–13 $\mu\text{m}$  data suffer from this problem. Because of their continuous wavelength coverage ISO-SWS01 spectra are well suited to shed more light on this question. In the following we will discuss this issue using the example of M82.

Firstly, evidence against a strong  $9.7\mu\text{m}$  absorption comes from the absence of a strong  $18\mu\text{m}$  silicate absorption (see Fig. 1). According to Draine & Lee (1984) the expected ratio  $\tau_{\text{sil}}(18\mu\text{m}) / \tau_{\text{sil}}(9.7\mu\text{m})$  is 0.4. Furthermore an analysis of hydrogen recombination lines in the ISO range yields a moderate  $A_V(\text{gas}) \approx 5$  mag (for a uniform screen model - see Schreiber 1998).

Next we come back to the comparison of the M82 spectrum to the spectrum of NGC 253 (Fig. 3). The two galaxies are similar in  $A_V$  and exhibit a very similar PAH spectrum. The only distinction appears to be a stronger VSG continuum in NGC 253. A strong rise of the continuum in this range is typical for regions of intense UV flux (e.g. Désert et al. 1990, Vigroux et al. 1996)<sup>3</sup>. The differ-

ence between both spectra can be well fit by a power-law continuum that begins to rise at approximately 8–9 $\mu\text{m}$ .

Finally, we compare our spectrum of M82 to the SWS01 spectrum of the galactic reflection nebula NGC 7023. Little extinction is expected in the line of sight to this nebula. The continuum under the PAH bands in NGC 7023 is very weak and starts to grow only beyond 20 $\mu\text{m}$  (Moutou et al. 1998). The flux density around 10 $\mu\text{m}$  is almost on the same level as the flux density shortward of the  $6\mu\text{m}$  PAH band and at 15–20 $\mu\text{m}$ . It could be explained by an underlying PAH plateau, or by the wings of the 7.7/8.6 and 11.3 PAH features (which can be represented by Lorentz profiles - Boulanger et al. 1998, Mattila et al. 1999). We therefore assume that in NGC 7023 this region consists mainly of emission bands, with little or no continuum and silicate absorption. In Fig. 4 we overplot the (smoothed) NGC 7023 spectrum on that of M82. The NGC 7023 spectrum has been multiplied by a factor 3.25 in order to normalize the PAH emission feature at  $7.6\mu\text{m}$  to the one in M82. The 3.3 and 11.3 $\mu\text{m}$  bands in M82 are weaker compared to NGC 7023. This might be explained e.g. by the harder radiation field in M82 (Joblin et al. 1996, see Sect. 4.2). Apart from this the two spectra are remarkably similar. Only at higher wavelengths a component of hot, small dust grains starts to add to the M82 continuum, as expected due to the much harder radiation field in M82.

In view of these arguments we constructed a toy model in order to reproduce the observed spectrum of M82. The model simply consists of the scaled spectrum of NGC 7023 plus a power-law continuum which starts at  $8.5\mu\text{m}$  ( $f \propto (\lambda - 8.5)^\alpha$ ). We use a power-law rather than a black body curve for sake of simplicity. A power-law produces a very good fit to the continuum up to 20 – 25 $\mu\text{m}$ . A black-body curve would be more problematic, because the dust may not have a single temperature, and might not be in thermal equilibrium. M82 is an extended source for the SWS apertures. There is a flux jump around 12 $\mu\text{m}$  by a factor of about 1.3, corresponding to a similar change in aperture size. We hence multiplied the power law continuum by 1.3 longward of 12 $\mu\text{m}$ <sup>4</sup>. The free parameters - the scaling factors for the NGC 7023 spectrum and the power law, plus the power law index - were adjusted by hand; we did not pursue a formal fit. Fig. 5 shows, that this simple model matches the observed spectrum remarkably well. There is no need to invoke any kind of extinction. Due to the uncertainties in the spectra, however, there is room for a moderate extinction, in accordance with the results from the recombination line studies ( $A_V \approx 5$  mag). A slightly different power-law, modified by a modest amount of extinction, could fit the spectrum equally well. However,

<sup>3</sup> The spectrum of NGC 253 indicates lower ionization (e.g. low [Ne III]/[Ne II]), but due to the compactness of the starburst in NGC 253 the radiation field here is more intense than in M82.

<sup>4</sup> A more accurate correction for the change in aperture size would have to assume a light distribution (as a function of wavelength) and a model of the instrument beam profile. Such a correction tool is not yet available.

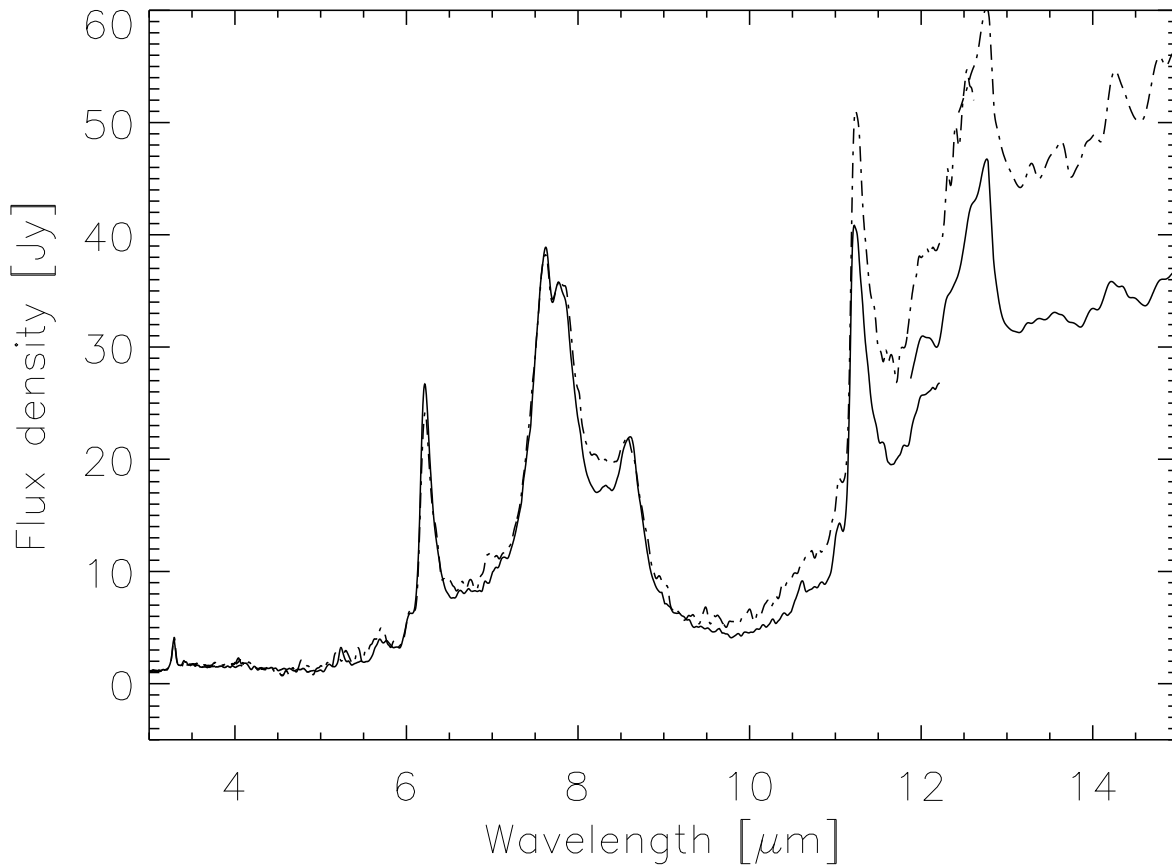


**Fig. 3.** M 82 (full) versus NGC 253 (dash-dotted). In both spectra narrow emission lines have been masked out. Both spectra have been smoothed and corrected for zodiacal light and for their red shift. The spectrum of NGC 253 has been multiplied by 2.6 to normalize the  $7.6\mu\text{m}$  PAH to the one in M 82.

a strong overall extinction, as deduced from the ground based  $8\text{--}13\mu\text{m}$  data ( $A_V = 15\text{--}60$  mag, Gillett et al. 1975), is clearly incompatible with the new ISO data. This is an example of the potential danger of overestimating the silicate absorption depth in baseline-limited data.

## 6. The interpretation of low resolution spectra

Many ISO spectra of galactic and extragalactic objects have been taken in low resolution mode (ISOPHOT-S, ISOCAM-CVF). Also, surveys with future mid- and far-infrared space missions, e.g. of galaxies at higher redshifts, will likely be performed with a relatively low resolution. For example the IRS spectrometer on board SIRTf will have a resolution of approximately 50–100 (plus a medium resolution mode of  $R=600$ ) in a wavelength range similar to ISO-SWS. In this low resolution mode SIRTf-IRS, being much more sensitive than ISO-SWS, will be a unique tool to detect emission features in spectra of faint high- $z$  galaxies. Low resolution spectra, however, suffer from pos-

sible identification and interpretation problems caused by coincidences of atomic/ionic lines and solid state features. In our high resolution SWS01 galaxy spectra lines and features are well separated, and we can use these spectra as templates to identify and highlight the importance of possible confusion problems. In Fig. 6 we have smoothed and rebinned the M 82 and NGC 1068 spectra to a resolution of 50 to simulate e.g. an ISOCAM-CVF or a SIRTf-IRS spectrum.

In Table 2 we have indicated possible confusions with nearby molecular, atomic, and ionic lines. We want to mention three lines in particular: [Ar II] at  $6.99\mu\text{m}$ , which might be confused with the underlying PAH emission (and the nearby  $\text{H}_2$  S(5) line), [Ne II] at  $12.8\mu\text{m}$ , which in fact has been confused in the past with the underlying  $12.7\mu\text{m}$  PAH feature, and [Ne V] at  $14.3\mu\text{m}$ , which also has been confused in the past with the nearby PAH emission. To get an indication of the relative contributions of the  $12.7\mu\text{m}$  PAH flux and the [Ne II] line flux to the combined (line plus feature) flux in low resolution spectra we have mea-

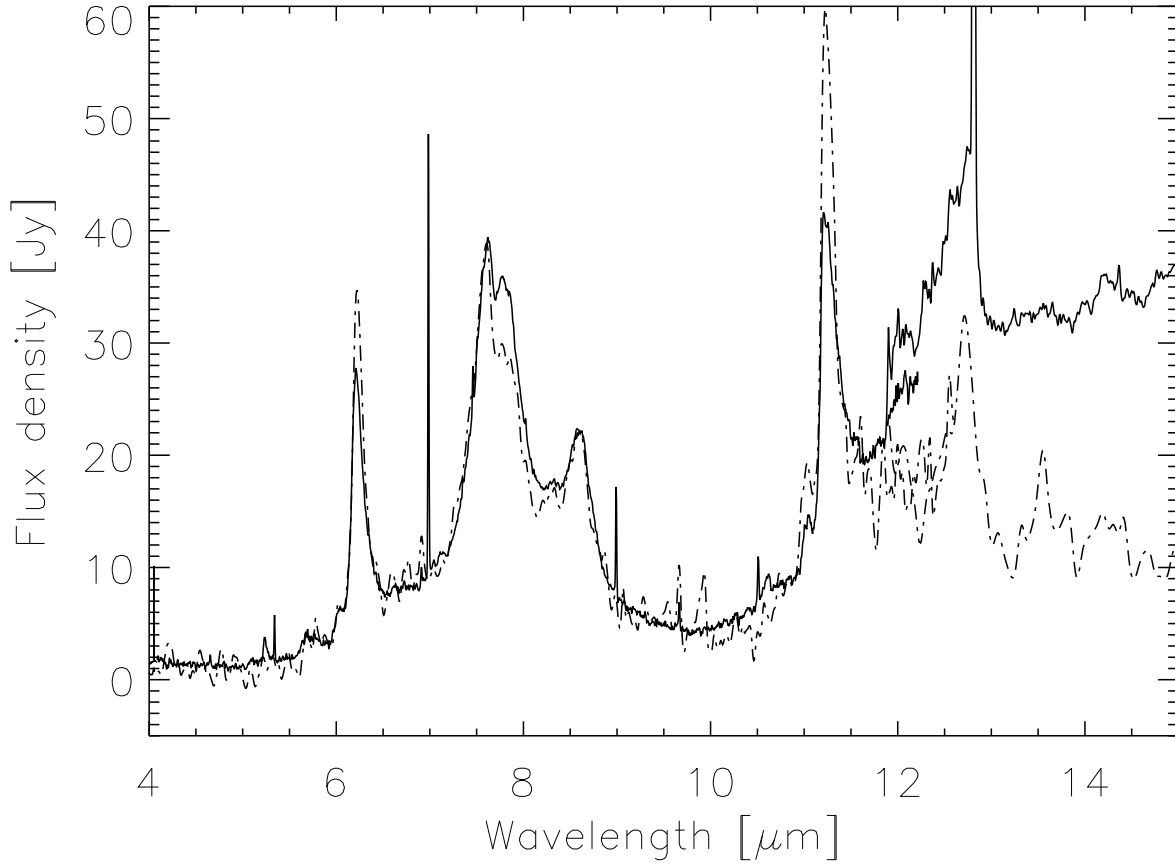


**Fig. 4.** M82 (full) versus the galactic reflection nebulae NGC 7023 (dash-dotted). Both spectra have been corrected for zodiacal light and for their red shift. The spectrum of NGC 7023 has been smoothed and multiplied by 3.25 to normalize the  $7.6\mu\text{m}$  PAH to the one in M82.

**Table 6.** The flux ratio of PAH 12.7 / [Ne II] 12.8

| Object   | PAH 12.7/[Ne II] 12.8 |
|----------|-----------------------|
| M82      | 0.96                  |
| NGC 253  | 1.32                  |
| 30 Dor   | 0.00                  |
| Circinus | 6.17                  |
| NGC 1068 | 0..1 <sup>a</sup>     |

<sup>a</sup> exact value difficult to measure, due to the broad wing of the [Ne II] line and the relatively strong noise.

sured both fluxes in our high resolution spectra. Table 6 summarizes the ratios of PAH/[Ne II] in all 5 templates. The values vary widely: in 30 Dor the flux is solely due to [Ne II], whereas in Circinus [Ne II] contributes only about 15% of the combined flux. For the  $7.0\mu\text{m}$  feature, we find that the broad feature contributes 25% of the combined flux of feature,  $\text{H}_2$ , and [Ar II] in NGC 253.

In the low resolution representation of M82 in Fig. 6 the shape of the  $14.3\mu\text{m}$  PAH resembles very much the shape of an unresolved line like the [Ne III] line at  $15.5\mu\text{m}$  and can be mistaken as [Ne V]. The high resolution spectrum of M82 (Fig. 2) clearly shows, that there is no [Ne V] at  $14.32\mu\text{m}$  but an emission feature plus a weak line of [Cl II]  $14.37\mu\text{m}$ . Of all the strong fine structure emission lines only few lines remain unambiguously detectable in low resolution spectra, like Br  $\beta$ , Br  $\alpha$ , [Ne III]  $15\mu\text{m}$ , [S III]  $18.7$ ,  $33.5\mu\text{m}$ , and [Si II]  $34.8\mu\text{m}$  in M82, or [O IV]  $26\mu\text{m}$  and perhaps [Ne V]  $24\mu\text{m}$ , and [S IV]  $10.5\mu\text{m}$  in NGC 1068. Clearly, low resolution spectra are very well suited for PAH and continuum measurements. However, flux measurements of narrow lines, and – in some cases – even their identification, can be very difficult. For these purposes higher resolutions, as for instance provided by the R=600 mode of the SIRTf spectrometer, are definitely needed.

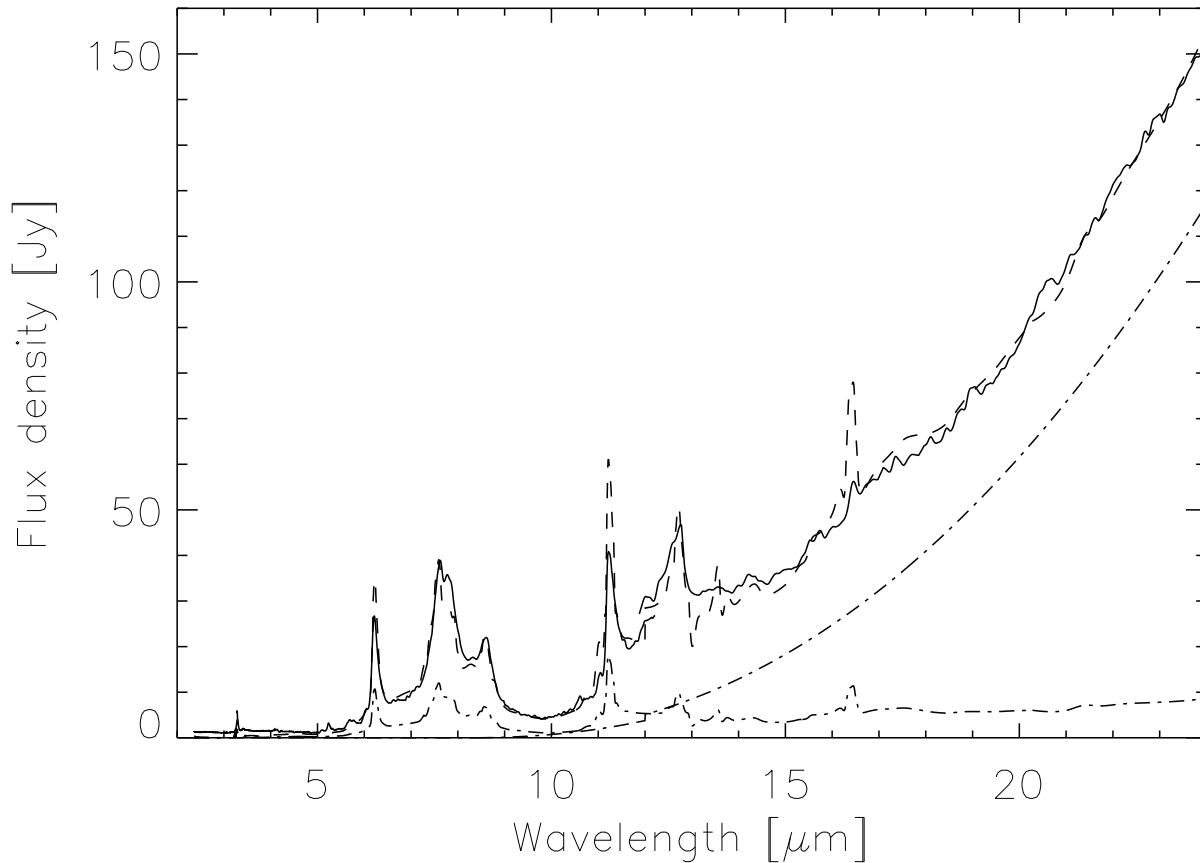


**Fig. 5.** M 82 (full) versus NGC 7023  $\times 3.25$  + power law (dashed). The spectra of NGC 7023 (dash-dotted) and M 82 have been smoothed. The power law component (dash-dotted) takes into account the aperture change at  $12\mu\text{m}$  ( $\times 1.3$ ).

## 7. Conclusions

We have detected a large number of mid-infrared features in galaxy spectra, some of them previously unobserved, and discussed the dependence of the dust features on ISM condition in galaxies. The spectral features vary considerably from source to source in presence and relative strength. Emission features are largely absent in the intense radiation field close to an AGN, and weak in a low metallicity, intensely star forming environment. Differences in the absorption spectra point to different physical properties of the obscuring regions in starburst and active galaxies.

The spectra presented here will be valuable template spectra for future mid- and far-infrared space missions such as SIRTf, SOFIA or FIRST. They provide important clues for the identification and interpretation of high redshift, dusty galaxies. The strongest PAH features can be used to provide redshift information in far-infrared photometric galaxy surveys (Simpson & Eisenhardt 1999, see also the example of 21396+3623, Rigopoulou et al. 1999). Furthermore, they affect galaxy number counts. For in-

stance, Xu et al. (1998) have constructed semi-empirical galaxy SEDs to model the considerable PAH effects on number counts and redshift distributions. Finally, the continuum and the PAH features can be used to distinguish between starburst activity and active nuclei in high redshift galaxies, as has been demonstrated for local infrared bright galaxies (Genzel et al. 1998, Lutz et al. 1998a, Rigopoulou et al. 1999).

The advantage of the wide wavelength coverage of the SWS spectra has been used to illustrate the problem of the continuum definition and the true depth of the silicate absorption. We find that in our starburst templates the hot VSG dust continuum begins to rise around 8 to  $9\mu\text{m}$ , and that it can be well fitted by a simple power-law up to  $20\text{--}25\mu\text{m}$ . Finally we have demonstrated possible line identification problems in low resolution spectra.

The spectra presented here are available in electronic form from the authors. We want to note again, that different parts of the spectra were observed through different aperture sizes, which should be taken into account for a detailed use as template spectra.

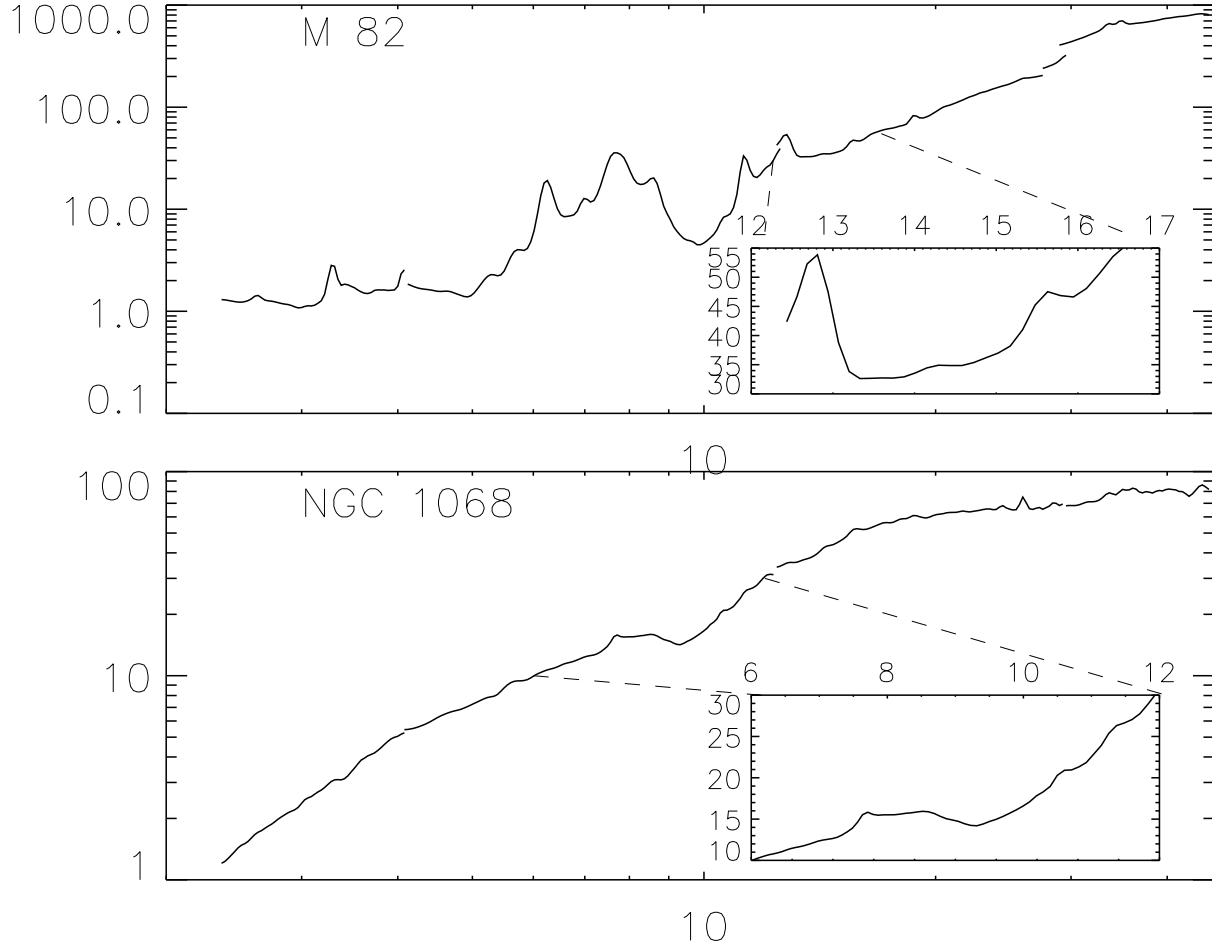


**Fig. 6.** The ISO-SWS spectra of M82 and NGC 1068, smoothed to a resolution of 50 to simulate the ISOCAM-CVF and SIRTf-IRS (low resolution mode) spectrometers. Wavelength in  $\mu\text{m}$ , flux density in Jansky. The feature at  $14.3\mu\text{m}$  in M82 is NOT [Ne V] (see text).

*Acknowledgements.* We wish to thank George Helou for very fruitful discussions, and Bernhard Brandl for support with the SIRTf-IRS simulations. SWS and the ISO Spectrometer Data Center at MPE are supported by DLR under grants 50 QI 8610 8 and 50 QI 9402 3. The ISO Spectral Analysis Package (ISAP) is a joint development by the LWS and SWS Instrument Teams and Data Centers. Contributing institutes are CESR, IAS, IPAC, MPE, RAL and SRON.

## References

- Beintema D. A., van den Ancker M.E., Molster F.J., et al. 1996, A&A 315, L369
- Boulanger F., Reach W. T., Abergel A., et al. 1996, A&A 315, L325
- Boulanger F., Boissel P., Cesarsky D., Rytter C. 1998, A&A 339, 194
- Bridger A., Wright G. S., Geballe T. R. 1994, in: I. McLean (ed.), *Infrared Astronomy with Arrays*, Dordrecht, Kluwer, p. 537
- Cesarsky D., Lequeux J., Abergel A., et al. 1996a, A&A 315, L305
- Cesarsky D., Lequeux J., Abergel A. et al. 1996b, A&A, 315, L309
- Chiar J. E., Tielens A. G. G. M., Whittet D. C. B., et al. 2000, submitted to ApJ
- Cohen M., Volk K. 1989, AJ 98, 1563
- Colbert J. W., Malkan M. A., Clegg P. E., et al. 1999, ApJ 511, 721
- Dartois E., Schutte W., Geballe T. R., et al. 1999, A&A 342, L32
- De Graauw T., Haser L. N., Beintema D. A., et al. 1996, A&A 315, L49
- Désert F.-X., Boulanger F., Puget J. L. 1990, A&A 237, 215
- D'Hendecourt L., Jourdain de Muizon M., Dartois E., et al. 1996, A&A 315, L365
- Draine B. T., Lee H. M. 1984, ApJ 285, 89
- Freedman W. L., Huhges S. M., Madore, B. F., et al. 1994, ApJ 427, 628
- García-Lario P., Manchado A., Ulla A., Manteiga M. 1999, ApJ 513, 941
- Genzel R., Lutz D., Sturm E., et al. 1998, ApJ 498, 579
- Gillett F. C., Kleinmann D. E., Wright E. L., Capps, R. W. 1975, ApJ 198, L65

- Helou G., Lu N., Werner M. W., Malhotra S., Silbermann N. 2000, submitted to ApJ
- Henning T., Begemann B., Mutschke H., Dorschner J. 1995, A&AS 112, 143
- Joblin C., Tielens A. G. G. M., Geballe T. R., Wooden, D. H. 1996, ApJ 460, L119
- Kessler M. F., Steinz J. A., Anderegg M.E., et al. 1996, ApJ 315, L27
- Lahuis F., Wieprecht E., Bauer O. H., et al. 1998, ASP Conf. Ser. 145: Astronomical Data Analysis Software and Systems VII, 7, 224
- Léger A., D'Hendecourt L., Defourneau D. 1989, ApJ 216, 148
- Lutz D., Feuchtgruber H., Genzel R., et al. 1996, A&A, 315, L269
- Lutz D., Spoon H. W. W., Rigopoulou D., Moorwood A. F. M., Genzel R. 1998a, ApJ 505, L103
- Lutz D., Genzel R., Kunze D., et al. 1998b, ASP Conf. Ser. 132: Star Formation with the Infrared Space Observatory, 89
- Lutz D., Sturm E., Genzel R., et al. 2000, submitted to ApJ
- Mattila K., Lehtinen K., Lemke D. 1999, A&A 342, 643
- Molster F.J., Waters L. B. F. M., Trams N. R., et al. 1999, A&A, in press (astro-ph/9908065)
- Moorwood A. F. M. 1986, A&A 166, 4
- Moorwood A. F. M., Glass I. S. 1984, A&A 135, 281
- Moorwood A. F. M., Lutz D., Oliva E., et al. 1996, A&A 315, L109
- Moutou C., Léger A., D'Hendecourt L. 1996, A&A 310, 297
- Moutou C., Sellgren K., Léger A., et al. 1998, ASP Conf. Ser. 132: Star Formation with the Infrared Space Observatory, 47
- Oliva E., Salvati M., Moorwood A. F. M., Marconi A. 1994, A&A 288, 457
- Oliva E., Marconi A., Cimatti A., Alighieri S. D. 1998, A&A 329, L21
- Packham C., Young S., Hough J. H., Axon D. J., Bailey J. A. 1997, MNRAS 288, 357
- Pier E. A., Krolik J. H. 1992, ApJ 401, 99
- Rigopoulou D., Spoon H. W. W., Genzel R., et al., 1999, AJ 118, 2625
- Roche P. F., Whitmore B., Aitken D. K., Phillips, M. M. 1984, MNRAS 207, 35
- Roche P. F., Aitken D. K., Smith C. H., Ward M. J. 1991, MNRAS, 248, 606
- Roelfsema P. R., Cox P., Tielens A.G. G. M., et al. 1996, A&A 315, L289
- Schreiber N. M. 1998, PhD Thesis, Ludwig-Maximilians-Universität München
- Simpson C., Eisenhardt P. 1999, PASP 111, 691
- Sturm E., Bauer O. H., Lutz D., et al. 1998, ASP Conf. Ser. 145: Astronomical Data Analysis Software and Systems VII, 7, 161
- Szczerba R., Henning Th., Volk K., Kwok S., Cox P. 1999, A&A 288, 457
- Thornley M. D., Lutz D., Kunze D., Spoon H. 1998, IAU Symposia 190, E110
- Tielens A. G. G. M., Hony S., van Kerckhoven C., Peeters E. 1999, in Proceedings of the Conference "The Universe as seen by ISO", Paris, France, 20-23 October 1998, P. Cox, M. Kessler (eds.), ESA SP-427
- Verstraete L., Puget J. L., Falgarone E., et al. 1996, A&A 315, L337
- Vigroux L., Mirabel F., Altieri B., et al. 1996, A&A 315, L93
- Volk K., Kwok S., Hrivnak B. J. 1999, ApJ 516, L99
- Voors R. H. M., Waters L. B. F. M., Morris P. W., et al. 1999, A&A 341, L67
- Waelkens C., Waters L. B. F. M., de Graauw M. S., et al. 1996, A&A 315, L245
- Waters L. B. F. M., Molster F.J., de Jong T., et al. 1996, A&A 315, L361
- Waters, L. B. F. M., Beintema D. A., Zijlstra A. A., et al. 1998, A&A 331, L61
- Webster A. 1995, MNRAS 277, 1555
- Whittet D. C. B., Schutte W. A., Tielens A. G. G. M. et al. 1996, A&A 315, L357
- Whittet D. C. B., Gerakines P. A., Tielens A. G. G. M., et al. 1998, ApJ 498, L159
- Wieprecht E., Lahuis F., Bauer O. H., et al. 1998, ASP Conf. Ser. 145: Astronomical Data Analysis Software and Systems VII, 7, 279
- Willner S. P., Soifer B. T., Russell R. W., Joyce R. R., Gillett F. C. 1977, ApJ 217, L121
- Witteborn F. C., Sandford S. A., Bregman J. D., et al. 1989, ApJ 341, 270
- Xu C., Hacking P. B., Fang F., et al. 1998, ApJ 508, 576